



***In silico* Screening of Potential Drug Candidate against Chain a of Coronavirus Binding Protein from Major Nigella Bioactive Compounds**

Md. Bokhtiar Rahman^{a,b*}, Simo^{a,c}, A.B.M Abdullah^{b,d}, Saba Tabassum^b and Toukir^b

^a Department of Biochemistry and Molecular Biology, Hajee Mohammad Danesh Science and Technology University, Dinajpur 5200, Bangladesh.

^b Research and Documentation Cell, Dushtha Shasthya Kendra (DSK), Dhaka 1207, Bangladesh.

^c Department of Pathology, Khulna Medical College Hospital, Khulna 9000, Bangladesh.

^d Department of Textile Engineering, Primeasia University, Dhaka 1207, Bangladesh.

Authors' contributions

This work was carried out in collaboration among all authors. Author MBR conceptualized and performed software work, visualization and wrote original draft. Author Simo contributed to methodology, supervision, validation, and also wrote original draft, and reviewed and edited the manuscript. Author ABMA checked validity, reviewed and edited the manuscript. Author ST reviewed and edited the manuscript and author Toukir also reviewed and edited the manuscript. All authors read and approved the final manuscript.

Article Information

DOI: <https://doi.org/10.9734/ajarr/2024/v18i7697>

Open Peer Review History:

This journal follows the Advanced Open Peer Review policy. Identity of the Reviewers, Editor(s) and additional Reviewers, peer review comments, different versions of the manuscript, comments of the editors, etc are available here: <https://www.sdiarticle5.com/review-history/117584>

Original Research Article

Received: 10/04/2024

Accepted: 14/06/2024

Published: 25/06/2024

*Corresponding author: Email: bokhtiarbdj@gmail.com; bokhtiar@dskbangladesh.org;

Cite as: Rahman, Md. Bokhtiar, Simo, A.B.M Abdullah, Saba Tabassum, and Toukir. 2024. "In Silico Screening of Potential Drug Candidate Against Chain a of Coronavirus Binding Protein from Major Nigella Bioactive Compounds". Asian Journal of Advanced Research and Reports 18 (7):224-38. <https://doi.org/10.9734/ajarr/2024/v18i7697>.

ABSTRACT

Background: More hazardous varieties of severe acute respiratory syndrome-related coronavirus have created major health hazards around the globe since 2019. There is no hundred percent effective drug has been developed against this virus. Bioactive compounds from plants are used as drugs or the main source of raw material for drugs against various diseases.

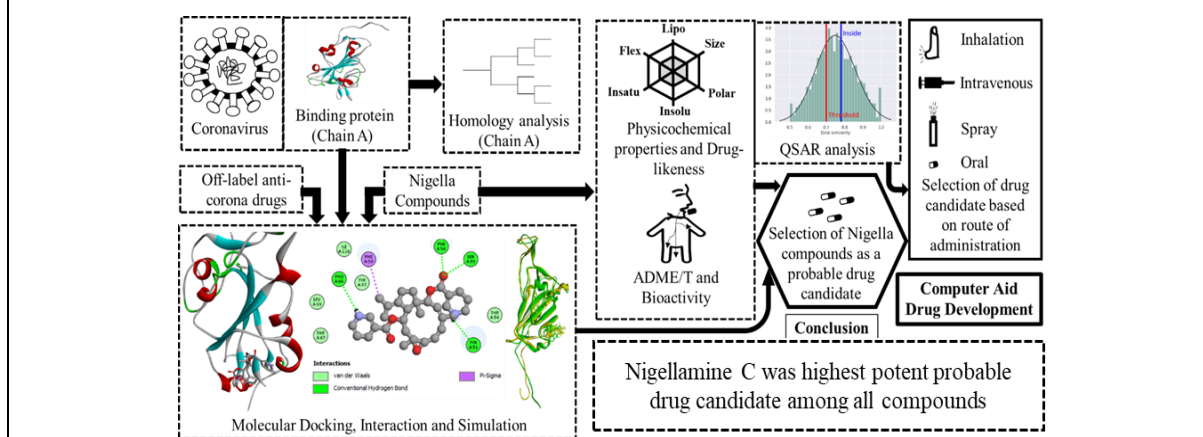
Aims: To screen the potential drug candidate against coronavirus from major Nigella bioactive compounds.

Methods and Materials: In the first step of our computational biology-dependent study, we selected six major Nigella compounds, four major drugs used in COVID-19 treatment, and a binding protein of coronavirus. In the second step, we processed the ligands and peptides and performed a docking to test the binding affinity. In the final step, we selected a compound with the highest binding affinity and performed molecular simulation, ADME/T, bioactivity, and QSAR analysis to characterize this molecule as a drug candidate.

Results: Four different antiviral agents that had been used in the treatment of COVID-19 patients showed less binding affinity in molecular docking compared with six bioactive compounds of Nigella. Nigellamine C, Nigeglanine, nigellamine D, nigellicine, nigellidine, and nigellone showed binding affinity of -7.9, -7.5, -7.3, -6.5, -7, and -6.7 kcal/mol, respectively whereas ribavirin, favipiravir, remdesivir, and nirmatrelvir showed -5.1, -4.8, -6.2, and -5.9 kcal/mol, accordingly to chain A of subunit 1 (S1) of the spike protein of coronavirus. Nigellamine C showed the highest binding affinity and suitable ADME/T properties with negligible toxic properties and good drug-likeness properties.

Conclusion: Nigellamine C may be a potent candidate for inhalation and/or oral drug development based on QSAR analysis and ADME/T analysis among all Nigella compounds.

Graphical Abstract



Keywords: Black cumin; phytochemicals; COVID-19; ADME/T; QSAR.

1. INTRODUCTION

Coronavirus is responsible for flu-like symptoms depending on the infectious disease with acute respiratory distress and an acute inflammatory state in humans [1]. The total number of cases and deaths during the COVID-19 pandemic was 676,609,955 and 6,881,955 from January 2020 to March 2023 worldwide [2]. Some therapeutic interventions such as convalescent plasma therapy, monoclonal antibodies therapy, immune response regulators, and some off-level drugs such as sotrovimab, regdanvimab, tocilizumab, infliximab, baricitinib, tofacitinib, ruxolitinib,

statins, anakinra, fluvoxamine, novaferon, remdesivir, ribavirin, favipiravir, molnupiravir, sofosbuvir, daclastivir, nirmatrelvir, ritonavir, etc. are used to treat its clinical complication [1]. However, there are no COVID-19 complete curing therapeutics or agents or drugs that can cure or prevent it from spreading.

More than 80% of the world's population relies on traditional medicinal plants for treating various illnesses [3] because medicinal plants are a good source of secondary metabolites that are used in multidisciplinary fields such as traditional systems of medicine, food supplements, modern

medicines, pharmaceutical products, folk medicines, and chemical industries [4]. Phytochemicals from black cumin may cure COVID-19 because traditionally oil of seeds from this plant was used in curing different symptoms associated with sinusitis such as coryza, nasal congestion, headache, neck pain, earache, and toothache since the ancient era [5]. It helps to inhibit the inflammation of sinuses and respiratory airways, and microbial infections as well as shows respiratory protective activities [6].

The traditional uses, phytochemical analysis, and biological activities of the black cumin seeds and their applications in human and animal health including poultry have been described in many literature and reviews [7-18]. Different extracts of this plant and seeds exhibited spasmolytic and bronchodilator activities [19], preventing early and late pulmonary fibrosis and inflammation [20] and showed anti-viral activity [21,22], anti-bacterial activity [21,23,24], anti-parasitic activity [25], anti-inflammatory activity [26-28], anti-allergic [29,30], anti-tumor activity [31-33], anti-oxidant activity [34,35], immune-modulatory activity [36], etc. It is high time to understand the interaction properties of nigella compounds to viral peptides for viral drug development. Thus, this computational biological method-dependent study aims to reveal the potential drug candidate against coronavirus from major Nigella bioactive compounds for helping future drug development.

2. MATERIAL AND METHODS

This in silico study has been designed to find out an effective metabolite that can help appropriate drug design against coronavirus-responsible disease. This study includes the following steps.

2.1 Protein Chain Selection and Properties Analysis

The S1 subunit C-domain serves as the RBD for most coronavirus. Chain A of this subunit plays a vital role in receptor binding and entry of various components of the virus into a cell. Chain A of spike protein S1 of coronavirus was searched in the NCBI protein databank (<https://www.ncbi.nlm.nih.gov/protein/242537309>). Chain A of Spike protein S1 (GI: 2425373090 and PDB: 7XNF) which was released on 2023-01-11 in the protein bank has been downloaded in FASTA format from NCBI. Physicochemical properties include the amino acids number, molecular weight, theoretical pI, aliphatic index, grand average of hydropathy (GRAVY),

Instability index, half-life, and charged residues number had been determined by using ProtParam analysis tools [37]. The function and family of this protein chain had been identified by the NCBI Conserved Protein Domain Family search tool (<https://www.ncbi.nlm.nih.gov/Structure/cdd/wrpsb.cgi>).

2.2 Homology Analysis and Phylogenetic Tree

Homology searching was carried out in NCBI blastp suite where the database was standard database of non-redundant protein sequences (nr) and the algorithm was blastp (protein-protein BLAST) (https://blast.ncbi.nlm.nih.gov/Blast.cgi?PROGRAM=blastp&PAGE_TYPE=BlastSearch&LINK_LOC=blasthome). Multiple sequence alignment and phylogenetic trees were made by using Molecular Evolutionary Genetics Analysis version 11 [38].

2.3 Structure Prediction and Validation of Chain A of Spike Protein S1

Various chemical and structural properties of secondary structure were predicted by using PSIPRED (<http://bioinf.cs.ucl.ac.uk/psipred/> &psipred_uuid=53bf5940-baf9-11ed-948f-00163e100d53) [39] and SOPMA (https://npsa-prabi.ibcp.fr/cgi-bin/npsa_automat.pl?page=/NPSA/npsa_sopma.html) [40] online tools.

2.4 Preparing and Validation of Macromolecule

The 3D structure of the target protein was determined using SWISS-MODEL web-based server (<https://swissmodel.expasy.org/interactive>) on homology modeling where the server automatically performs BLASTp search to identify templates for each protein sequence [41]. The Cryo-EM structure of PCoV_GX Spike glycoprotein A was selected for homology modeling from the searched result. The identification of the sequence was 100%, the GMQE value was 0.85, the QSQE value was 0.60, the method was EM and the oligo-state was homo-trimer. This modeled homo-trimer peptide was analyzed by PROCHECK [42] (Job ID: 1279619) and ProSA [43, 44]. The 3D model structure was visualized by BIOVIA Discovery Studio Visualizer [45] and deleted chain B, Chain C, and attached ligands. No water molecule was found. Polarized the remained chain A monomer by BIOVIA Discovery Studio Visualizer and analyzed again by PROCHECK (Job ID: 1279624).

2.5 Ligand Selection and Preparation

Six major metabolites of *N. sativa* were selected and the 3D structures of these compounds were downloaded as SDF files (.sdf) from PubChem (<https://pubchem.ncbi.nlm.nih.gov/>). All six compounds were nigeplanine (PubChem CID 12116700), nigellamine C (PubChem CID 101341399), nigellamine D (PubChem CID 101727452), nigellicine (PubChem CID 11402337), nigellidine (PubChem CID 136828302) and nigellone (PubChem CID 398941). Four different antiviral therapeutic agents that are commonly used in COVID-19 off-level treatment were also selected for comparison after the deep literature review [1]. The 3D structures of these therapeutic drugs were also downloaded as SDF files (.sdf) from PubChem named ribavirin (PubChem CID 37542), favipiravir (PubChem CID 492405), remdesivir (PubChem CID121304016) and nirmatrelvir (PubChem CID155903259). All compounds were converted from SDF files (.sdf) file to the PDB format (.pdb) using the Open Babel graphical user interface (GUI) tool [46]. The energy minimization of all ligands and control drugs was performed by using PyRx tool [47].

2.6 Molecular Docking and Simulation

The conversion from the PDB files (.pdb) to the PDBQT files (.pdbqt) format and the molecular docking of individual ligands into the target chain A of spike protein S1 was performed by using the PyRx tool [47]. Vina search space was maximized for macromolecule in Pyrax where the center was X: 164.3046, Y: 177.8894, and Z: 202.6309, and the dimension (angstrom) was X: 69.4436, Y: 41.6859, and Z: 67.7703. Molecular dynamics simulation was done by using myPresto version 5 [48]. Crystal water solvate was used, the system size was a sphere, and the margins (A) were 8 margins from molecular size. Center coordination was the center of gravity of the molecule and the ion was automatically neutralized. Hydrogen atoms were added to the ligands and the partial charge was also added by the Gasteiger method.

2.7 ADME/T and Bioactivity Analysis in Human

The ADME was predicted using SwissADME [49] and pKCSM [50] web-based molecular tools. Lipinski, ≤ 10 , NH or OH ≤ 5 [51]; Ghose,

molecular weight was between 160 and 480 Da, WlogP is between -0.4 to 5.6, molar refractivity (MR) was between 40 to 130 for the total number of atoms; the qualifying range was between 20 and 70 atoms in a small molecule [52, 53]; Veber, ≤ 10 rotatable bonds and a TPSA equal to or less than 140 Å² with 12 or fewer H-bond donors and acceptor [54]; Egan, WLOGP ≤ 5.88 and TPSA ≤ 131.6 , respectively [55]; Muegge, molecular weight between 200 to 600 Da, XLOGP between -2 and 5, TPSA ≤ 150 , number of rings ≤ 7 , number of carbon atoms > 4 , number of heteroatoms > 1 , number of rotatable bonds ≤ 15 , H-bond acceptor ≤ 10 , H-bond donor ≤ 5 [56]; and bioavailability score, $F > 10\%$ [57]. Medicinal chemistry friendliness was predicted by PAINS [58], Brenk [59], lead-likeness [60], and synthetic accessibility (from 1 is very easy to 10 is very difficult) methods. The Molinspiration server was used to evaluate the biological activities where the bioactivity score < -5.0 is regarded as a biologically inactive compound, -5.0 to < 0 as a moderately active compound, and > 0 is regarded as a biologically active compound [61]. ProTox-II server was used to evaluate the toxicity of the compound [62].

2.8 QSAR Model Using Powerful Machine Learning Algorithm

SToxTox web portal was used to identify hazardous potentiality in QSAR (Quantitative Structure-Activity Relationships) model [63]. The acute toxicity tests included acute oral toxicity (OECD TG 401, 420, 423, and 425 and compounds 8495) in the rat model, acute dermal toxicity (OECD TG 402 and compounds 1884) in rabbit and rat models, acute inhalation toxicity (OECD TG 403 and 436 and compounds 681), skin irritation and corrosion (OECD TG 404 and compounds 1012) by Draize test in the rabbit model, eye irritation and corrosion (OECD TG 405 and compounds 3547) via Draize test in the rabbit model and skin sensitization (OECD TG 429 and 442 and compounds 1000) via LLNA test in mouse and guinea pig. Random Forest was the machine-learning algorithm for all tests. The predicted fragment contribution of toxic effects was accompanied by the map of the atomic contributions to toxicity where the red regions with continuous lines indicated the fragment was predicted to increase toxicity and green regions with dashed lines indicated the fragment was predicted to decrease toxicity.

3. RESULTS AND DISCUSSION

3.1 Protein Chain Selection and Properties of Chain A

Chain A (GI: 2425373090) is a receptor-binding domain (RBD) of the S1 subunit of severe acute respiratory syndrome coronavirus 2 spike (S) proteins (superfamily member cd21480). According to NCBI Conserved Protein Domain Family, this part plays the most important role in viral attachment, fusion, and entry into host cells, and serves as a major target for the development of neutralizing antibodies, inhibitors of viral entry, and vaccines. The general properties were pssm-Id.: 424109, Cd length: 223, bit score: 394.08, and e-value: 1.91e-141. The physicochemical properties of Chain A from S1 subunit C-domain included the amino acids: 215, molecular weight: 24210.41, theoretical pI: 8.73, aliphatic index: 73.81, grand average of hydropathicity (GRAVY): -0.230, instability index: 19.43 and stable, estimated half-life: 1 hours (mammalian, reticulocytes, in vitro), total number of negatively charged residues (Asp + Glu): 15 and total number of positively charged residues (Arg + Lys): 20.

3.2 Homology Analysis and Phylogenetic Tree

Homology analysis and phylogenetic tree from NCBI blastp proved that the segment of Chain A from S1 subunit one was a part of the coronavirus glycoprotein family (Fig. 1.) where the homology method was

MUSCLE, the statistical method was neighbor-joining and the bootstrap replications was 1000.

3.3 Structure Prediction of Chain A of Spike Protein S1

The secondary structure of chain A of spike protein S1 of coronavirus was analyzed by PSIPRED and SOPMA (Id.: 9254fa70e19f, started: 20230313-075340 and name: chainx0 A of Spike protein S1). The analysis results of PSIPRED are visualized in Fig. 2. In SOPMA, the random coil was found to be the most predominant at 56.28% followed by extended strand, alpha helix, and beta-turn were 27.44, 9.30, and 6.98 %, respectively.

3.4 Preparing and Validation of Macromolecule

The 3D model of the Cryo-EM structure of PCoV_GX spike glycoprotein A and the cleaned polarized chain A of spike protein S1 is given in Fig. 3. The summary of Ramachandran plots of the Cryo-EM structure of PCoV_GX spike glycoprotein A and the cleaned polarized chain A of spike protein S1 of coronavirus are given in Table 1. The percent of amino acid residues of the Cryo-EM structure of PCoV_GX spike glycoprotein A and the chain A of spike protein S1 fell within the most favored region in the "Ramachandran plot" based on PROCHECK result. In ProSA, the amino acid number was 209 and the Z score was 5.97.

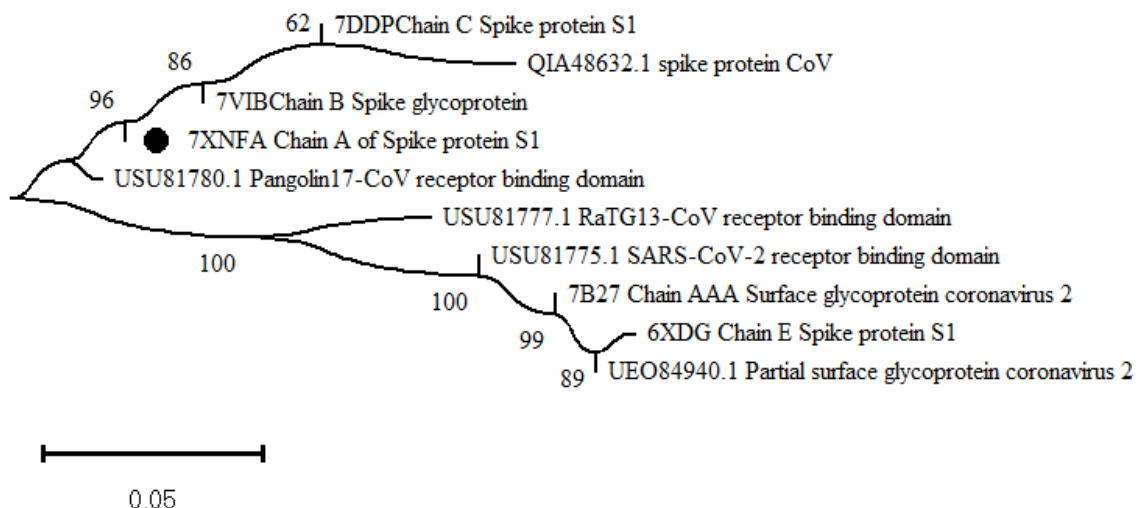


Fig. 1. Phylogenetic tree of chain A from S1 subunit and other related protein parts

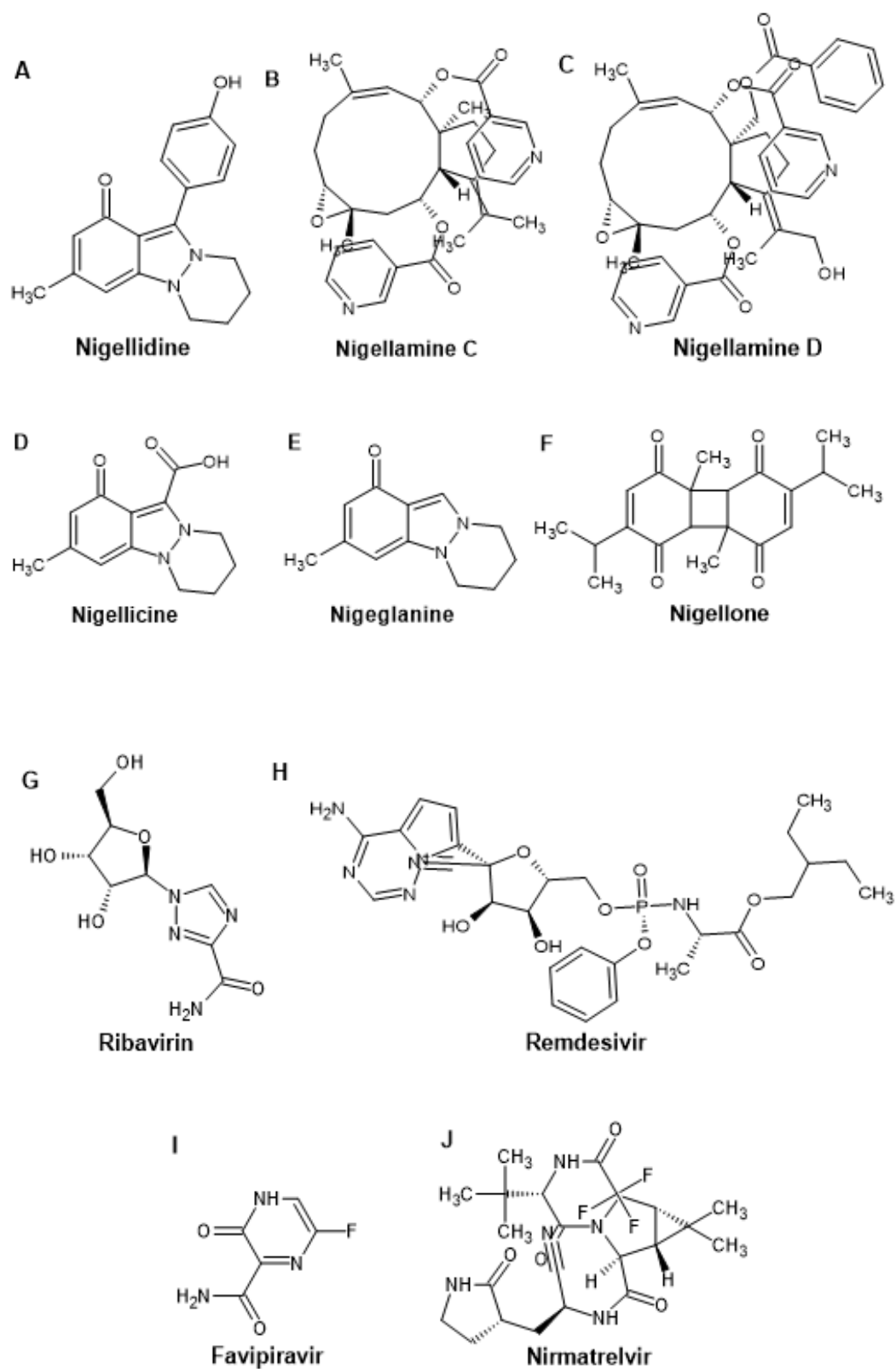


Fig. 4. 2D chemical structure of different metabolites and commonly used COVID-19 therapeutics

Table 2. Details of binding affinity and interaction between chain A and ligands

Compound name	Molecular formula	Molecular weight	Binding affinity (kcal/mol)	Residue in contact	Interaction type	Distance				
Nigeglanine	C ₁₂ H ₁₄ N ₂ O	202.25	7.5	-	CYS18	Alkyl	4.58597			
				ILE40	Alkyl	4.80409				
				ALA45	Alkyl	4.49616				
				VAL77	Alkyl	4.34818				
				LEU195	Alkyl	5.03289				
				VAL206	Alkyl	5.3736				
				LEU50	Alkyl	4.95935				
				ILE116	Alkyl	4.8034				
				PHE24	Pi-Alkyl	4.6959				
				PHE56	Pi-Alkyl	5.38877				
				ALA45	Pi-Alkyl	4.40149				
				LEU195	Pi-Alkyl	4.80967				
				LEU195	Pi-Alkyl	5.21649				
				TYR47	Pi-Pi Stacked	5.54815				
				Nigellamine C	C ₃₂ H ₃₈ N ₂ O ₅	530.7	-7.9	SER55	Hydrogen Bond	2.40719
PHE56	Hydrogen Bond	2.1157								
PRO66	Hydrogen Bond	2.94736								
TYR51	Hydrogen Bond	2.24315								
PHE59	Pi-Sigma	3.57235								
Nigellamine D	C ₃₉ H ₄₂ N ₂ O ₈	666.8	-7.3	SER55	Hydrogen Bond	2.35783				
				PHE59	Hydrogen Bond	2.52482				
				TYR51	Hydrogen Bond	2.47743				
				THR54	Hydrogen Bond	2.82209				
				PRO66	Hydrogen Bond	2.89098				
Nigellicine	C ₁₃ H ₁₄ N ₂ O ₃	246.26	-6.5	THR54	Hydrogen Bond	2.31726				
				PHE56	Pi-Pi T-shaped	5.00223				
				PHE59	Pi-Pi T-shaped	4.95843				
				PHE59	Pi-Pi T-shaped	5.60944				
				TYR47	Pi-Alkyl	4.14739				
Nigellidine	C ₁₈ H ₁₈ N ₂ O ₂	294.3	-7	TYR51	Hydrogen Bond	2.83052				
				TYR47	Pi-Pi Stacked	5.40681				
				TYR51	Pi-Pi Stacked	5.33247				
				PHE59	Pi-Pi T-shaped	4.73143				
				PHE59	Pi-Pi T-shaped	5.44998				
				TYR47	Pi-Alkyl	4.00084				
				PHE59	Pi-Alkyl	4.11259				
Nigellone	C ₂₀ H ₂₄ O ₄	328.4	-6.7	TYR51	Hydrogen Bond	2.28764				
				Ribavirin	C ₈ H ₁₂ N ₄ O ₅	244.20	-5.1	PHE56	Hydrogen Bond	1.94621
								THR54	Hydrogen Bond	2.35982
Favipiravir	C ₅ H ₄ FN ₃ O ₂	157.10	-4.8	CYS18	Pi-Sulfur	5.79321				
				PHE74	Pi-Pi Stacked	4.52437				
				ALA45	Pi-Alkyl	4.00721				
				VAL77	Pi-Alkyl	5.27546				
				LEU195	Pi-Alkyl	5.0039				
Remdesivir	C ₂₇ H ₃₅ N ₆ O ₈ P	602.6	-6.2	TYR51	Hydrogen Bond	2.25127				
				THR54	Hydrogen Bond	2.62554				
				TYR51	Hydrogen Bond	2.15073				
				TYR47	Pi-Pi Stacked	5.27052				
				PHE56	Pi-Pi T-shaped	5.00422				
				PHE59	Pi-Pi T-shaped	4.78039				
				TYR51	Pi-Alkyl	4.95075				
Nirmatrelvir	C ₂₃ H ₃₂ F ₃ N ₅ O ₄	499.5	-5.9	THR58	Hydrogen Bond	2.34192				
				ARG90	Hydrogen Bond	2.33035				
				GLY86	Hydrogen Bond	1.80821				

3.5 Nigella Compounds and Available Therapeutic Drugs against COVID-19

The 2D structures of selected phytochemicals such as nigeplanine, nigellamine C, nigellamine D, nigellicine, nigellidine, and nigellone as ligands and selected therapeutic drugs such as ribavirin, favipiravir, remdesivir, and nirmatrelvir are given in Fig. 4.

3.6 Binding Affinity and Interaction between Chain A and Major Nigella Compounds

Identification of non-covalent interactions such as hydrophobic contacts, hydrogen bonds, salt bridges, etc., and the nature of the interaction of bioactive molecules with their target is very important in drug design because these are stabilizing factors of target-ligand interaction [64]. All six selected compounds from *N. Sativa* showed potent binding affinity against chain A of spike protein S1 of SARS-CoV-2 (Table 2). Among them, nigellamine C showed the highest binding affinity of -7.9 kcal/mol where the

contact residues were CYS18, ILE40, ALA45, VAL77, LEU195, VAL206, LEU50, ILE116, PHE24, PHE56, ALA45, LEU195, LEU195, TYR47 (Fig. 5). Four different antiviral agents that had been used in the treatment of COVID-19 patients showed less binding affinity compared with these bioactive compounds of *Nigella*. Nigeplanine, nigellamine D, nigellicine, nigellidine, and nigellone showed binding affinity of -7.5, -7.3, -6.5, -7, and -6.7 kcal/mol, respectively whereas ribavirin, favipiravir, remdesivir, and nirmatrelvir showed -5.1, -4.8, -6.2, and -5.9 kcal/mol, accordingly (Table 2). Nigeplanine, nigellicine, and nigellidine showed mostly hydrophobic interaction while nigellamine C, nigellamine D, and nigellone showed conventional hydrogen bond interaction.

The 3D surface view, 3D tube pose view, H bond donor and acceptor scenario, 3D protein-ligand binding interaction, and 2D protein-ligand binding interaction of nigellamine C are given in Fig. 6. Nigellamine C was selected for further analysis because of its highest binding affinity and the presence of hydrogen bonds.

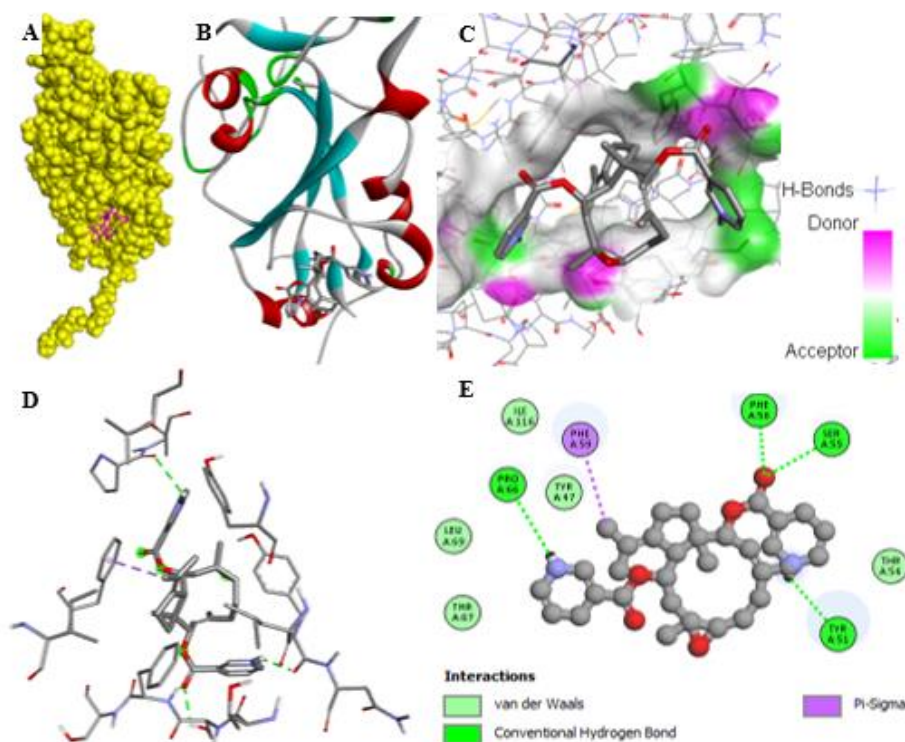


Fig. 5. Binding modes for the nigellamine C within the active site of the chain A of the spike protein of coronavirus: (A) 3D surface view; (B) 3D tube pose view; (C) Hydrogen bond donor and acceptor; (D) 3D protein-ligand binding interaction and (E) 2D protein-ligand binding interaction

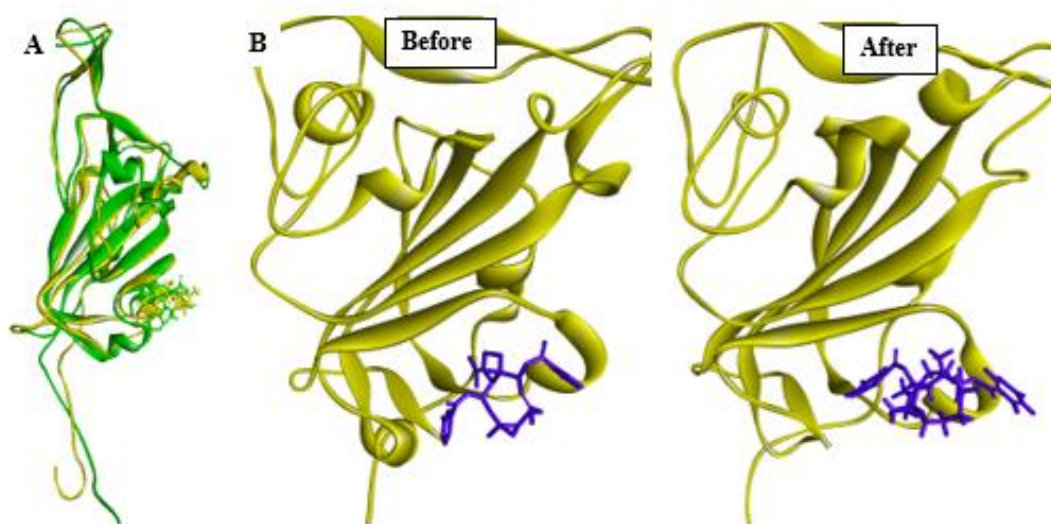


Fig. 6. The superimposed structure of pre and post-molecular dynamics simulation nigellamine C. (A) The yellow color denotes the pre-molecular dynamics structure, and the green color denotes the post-molecular dynamics structure, and (B) comparing surface view between the initial and final structures of the complexes from MD simulations at the snapshot of 4 psec

Table 3. ADME Properties of the Selected Phytochemicals

ADME properties		Other properties	
(a) Absorption		(a) Biological activities	
Water solubility (log mol/L)	-4.664	GPCR ligand	-0.00
Intestinal absorption in human (%)	98.377	Ion channel modulator	-0.19
Skin Permeability (log Kp)	-2.762	Kinase inhibitor	-0.39
P-glycoprotein substrate	No	Nuclear receptor ligand	0.31
(b) Distribution		Protease inhibitor	0.04
VDss in humans (log L/kg)	0.12	Enzyme inhibitor	0.31
Fraction unbound in humans (Fu)	0	(b) Druglikeness	
BBB permeability (log BB)	-0.799	Lipinski	Yes; 1 violation: MW>500
CNS permeability (log PS)	-2.957	Ghose	No; 4 violations: MW>480, WLOGP>5.6, MR>130, #atoms>70
(c) Metabolism		Veber	Yes
CYP2D6 substrate	No	Egan	No; 1 violation: WLOGP>5.88
CYP3A4 substrate	Yes	Muegge	Yes
CYP1A2 inhibitor	No	Bioavailability score	0.55
CYP2C19, CYP2C9 and CYP2D6 inhibitor	No	(c) Medicinal chemistry	
CYP3A4 inhibitor	Yes	PAINS	0 alert
(d) Excretion		Brenk	3 alerts: Three-embered_heterocycle, isolated_alkene, more_than_2_esters
Total Clearance (log ml/min/kg)	0.37	Leadlikeness	No; 2 violations: MW>350, XLOGP3>3.5
Renal OCT2 substrate	No	Synthetic accessibility	6.05

The superimposed structure of pre and post-molecular dynamics simulation of the protein-ligands complex is given in Fig. 6A. Comparison between the surface view of initial and final

structures of the complexes from MD simulations at the snapshot of 4 psec are presented in Fig. 6B. The nigellamine C was in the same pocket after molecular simulation.

3.7 ADME/T and Bioactivity Analysis

Absorption, distribution, metabolism, excretion, and toxicity properties together are called ADME-Tox properties prediction and play an important role in drug development because they account for the failure of 60% of drug molecules during the drug development process [65]. Thus, cost-effective in-silico tools early prediction of ADME analysis of nigellamine C is given in Table 3 where the intestinal absorption property was 98%, and the total clearance amounts was 0.37 log ml/min/kg. Physicochemical properties and lipophilicity were also predicted via SMILES where the TPSA (the polar surface area) was 90.91 Å² and the consensus log Po/w was 4.80 for nigellamine C.

Biological activities, drug-likeness, and medicinal properties of nigellamine C are given in (Table 3) where positive drug-likeness properties were shown in all models Lipinski, Ghose, Veber, Egan, and Muegge and the bioavailability score was 0.55. Nigellamine C showed 0 alerts in PAINS but 3 alerts in the Brenk assay and a negative response in the lead likeness assay.

The synthetic accessibility score was 6.05. Nigellamine C belongs to the toxicity class 6. The LD50 value was 10000 mg/kg.

Nigellamine C showed inactive in hepatotoxicity, mutagenicity, and cytotoxicity as well as inactive in important targets such as aryl hydrocarbon receptor (AhR), androgen receptor (AR), androgen receptor ligand binding domain (AR-LBD), aromatase estrogen Receptor Alpha (ER), estrogen receptor ligand binding domain (ER-LBD), peroxisome proliferator-activated receptor gamma (PPAR-Gamma), nuclear factor (erythroid-derived 2)-like 2/antioxidant responsive element (nrf2/ARE), heat shock factor response element (HSE), phosphoprotein (tumor suppressor) p53 and ATPase family AAA domain-containing protein 5 (ATAD5).

3.8 QSAR Analysis

Nigellamine C did not produce any acute systemic and topical toxicity nature in the QSAR model where the confidence level of all tests was ≥ 50% Fig. 7.

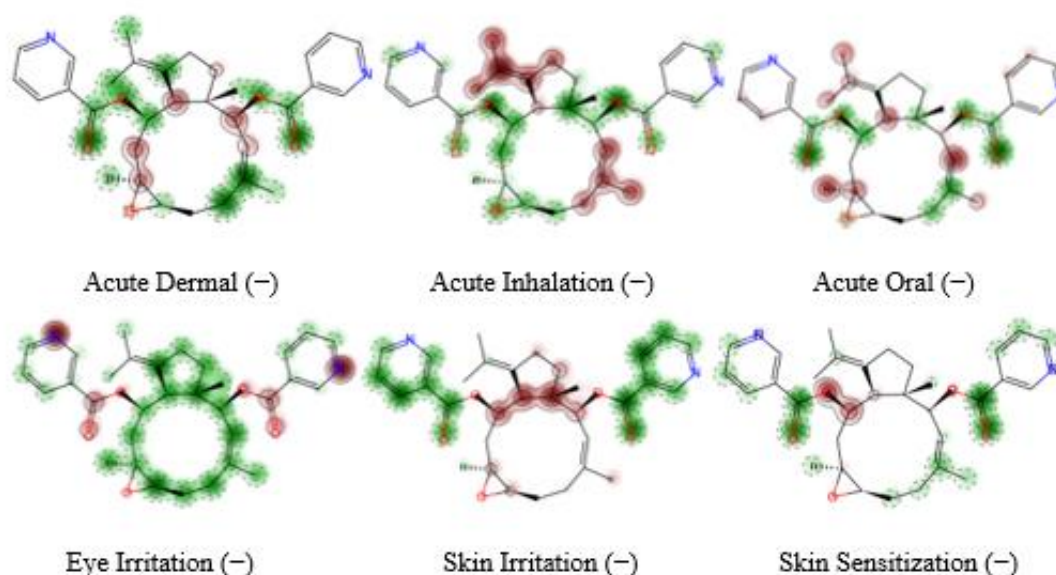


Fig. 7. Maps of fragment contributions and predictions of Nigellamine C. (Red regions with continuous lines indicate the fragment is predicted to increase toxicity, the green regions with dashed lines indicate the fragment is predicted to decrease toxicity and the gray isolines define the frontier between the positive (red) and the negative (green) contributions. (+) denotes the toxic and (-) denotes the non-toxic nature)

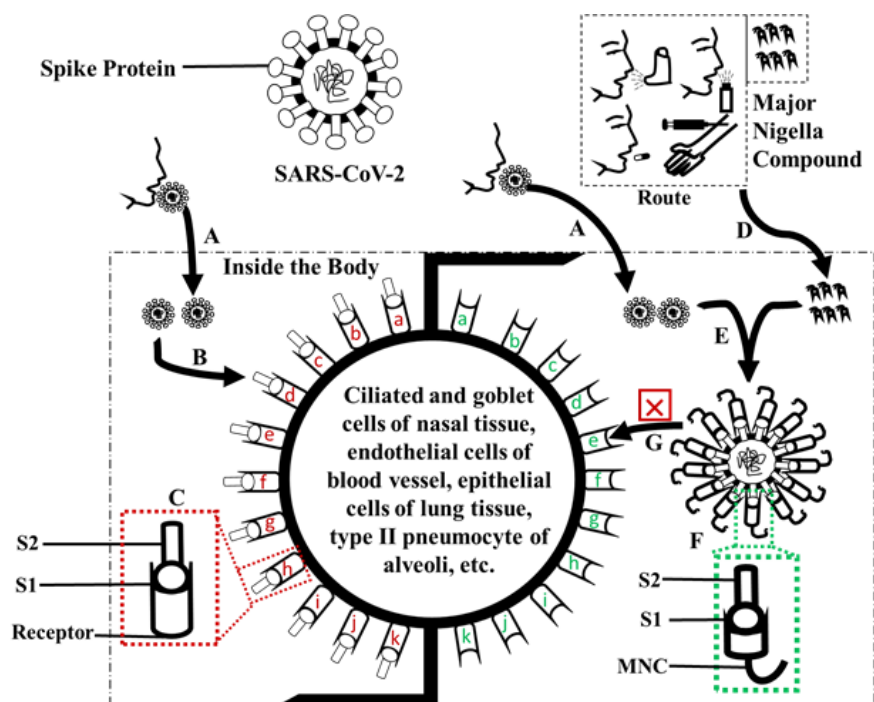


Fig. 8. Probable mode of action of Nigellamine C as a drug candidate

3.9 Summary of Results and Probable Mode of Action of Nigellamine C

Compared with the COVID-19 drugs ribavirin, favipiravir, remdesivir and nirmatrelvir with nigellamine C showed more binding affinity against chain A of the spike protein of coronavirus in molecular docking analysis. Nigellamine C also proved itself as a probable potential drug candidate in ADME/T and QSAR analysis. It can be considered for inhalation and oral drug development. Generally, coronavirus binds to ACE-2 (Angiotensin-converting enzyme 2), heparan sulfate, sialic acid receptor of ciliated cells in nasal tissue cells, CD147, GRP78 (glucose-regulating protein 78), lectins (CD209L/CD209), and integrins of epithelial cells of lung tissue, DPP4 (dipeptidyl peptidase-4)/CD26 endothelial cells of the blood vessel, vimentin of pneumocyte of alveoli, NRP-1 (neuropilin-1) in epithelial cells in the olfactory tissue and bone marrow-derived macrophages, AXL (tyrosine-protein kinase receptor) of pulmonary epithelia [66]. A probable mode of action of nigellamine C (MNC) is given in Fig. 8.

4. CONCLUSION

Pharmaceutical industries, food and ornamental industries, medicine, chemical industries, and research laboratories give attention to traditional medicinal plants because these are the sources

of bioactive natural compounds. Nigellamine C has proved itself as a more potent antiviral drug candidate among other compounds based on molecular docking, ADME/T, and QSAR analysis. This study will help in advancing phytochemical-dependent antiviral drug development in the future.

DISCLAIMER (ARTIFICIAL INTELLIGENCE)

Author(s) hereby declare that NO generative AI technologies such as Large Language Models (ChatGPT, COPILOT, etc) and text-to-image generators have been used during writing or editing of manuscripts.

ACKNOWLEDGMENTS

Authors are highly acknowledged by the Department of Biochemistry and Molecular Biology, Hajee Mohammad Danesh Science and Technology University, Dinajpur, Bangladesh; Research and Documentation Cell, Dushtha Shasthya Kendra (DSK), Dhaka, Bangladesh; and Department of Pathology, Khulna Medical College Hospital, Khulna, Bangladesh for give the platform and opportunity to do this study.

COMPETING INTERESTS

Authors have declared that no competing interests exist.

REFERENCES

- Bischof E, Wolfe J, Klein SL. Clinical trials for COVID-19 should include sex as a variable. *The Journal of Clinical Investigation*. 2020;130(7):3350-3352.
- JHCRC JHCRC. COVID-19 Map. Johns Hopkins Coronavirus Resource Center; 2023.
- Akerele O. Nature's medicinal bounty: Don't throw it away. *World Health Forum*. 1993;14:390-395.
- Karna S. Phytochemical screening and gas chromatography–mass spectrometry and analysis of seed extract of *N. sativa*, Linn. *International Journal of Chemical Studies*. 2013;1(4):183-188.
- Mahboubi M. Natural therapeutic approach of *N. sativa* (Black seed) fixed oil in management of Sinusitis. *Integrative Medicine Research*. 2018;7(1):27-32.
- El Tahir KE, Ashour MM, Al-Harbi MM. The respiratory effects of the volatile oil of the black seed (*N. Sativa*) in guinea-pigs: Elucidation of the mechanism (s) of action. *General Pharmacology: The Vascular System*. 1993;24(5):1115-1122.
- Ahmad A, et al. A review on therapeutic potential of *N. Sativa*: A miracle herb. *Asian Pacific Journal of Tropical Biomedicine*. 2013;3(5):337-352.
- Azeem T, et al. Effect of *N. Sativa* on poultry health and production: A review. *Science Letter*. 2014;2(2):76-82.
- Forouzanfar F, Bazzaz BSF, Hosseinzadeh H. Black cummin (*N. sativa*) and its constituent (thymoquinone): A review on antimicrobial effects. *Iranian Journal of Basic Medical Sciences*. 2014; 17(12):929.
- Gilani AUH, Jabeen Q, Khan MAU. A review of medicinal uses and pharmacological activities of *N. sativa*. *Pakistan Journal of Biological Sciences*. 2004;7(4):441-5.
- Kooti W, et al. Phytochemistry, pharmacology, and therapeutic uses of black seed (*N. sativa*). *Chinese Journal of Natural Medicines*. 2016;14(10):732-745.
- Majdalawieh AF, Fayyad MW. Immunomodulatory and anti-inflammatory action of *N. sativa* and thymoquinone: A comprehensive review. *International Immunopharmacology*. 2015;28(1):295-304.
- Mollazadeh H, Hosseinzadeh H. The protective effect of *N. sativa* against liver injury: A review. *Iranian Journal of Basic Medical Sciences*. 2014;17(12):958.
- Paarakh PM. *N. sativa* Linn.—A comprehensive review; 2010.
- Ragheb A, et al. The protective effect of thymoquinone, an anti-oxidant and anti-inflammatory agent, against renal injury: A review. *Saudi Journal of Kidney Diseases and Transplantation*. 2009;20(5):741.
- Randhawa MA, Alghamdi MS. Anticancer activity of *N. sativa* (black seed)—a review. *The American Journal of Chinese Medicine*. 2011;39(06):1075-1091.
- Sharma N, et al. Medicinal and pharmacological potential of *N. sativa*: A review. *Ethnobotanical Leaflets*. 2009; 2009(7):11.
- Tembhurne S, et al. A review on therapeutic potential of *N. sativa* (*kalonji*) seeds. *Journal of Medicinal Plants Research*. 2014;8(3):167-177.
- Gilani A, et al. Bronchodilator, spasmolytic and calcium antagonist activities of *N. sativa* seeds (*Kalonji*): A traditional herbal product with multiple medicinal uses. *The Journal of the Pakistan Medical Association*. 2001;51(3):115-120.
- Poursalehi HR, et al. Early and late preventive effect of *N. sativa* on the bleomycin-induced pulmonary fibrosis in rats: An experimental study. *Avicenna Journal of Phytomedicine*. 2018;8(3):263.
- Hanafy M, Hatem M. Studies on the antimicrobial activity of *Nigella sativa* seed (*black cummin*). *Journal of Ethnopharmacology*. 1991;34(2-3):275-278.
- Salem ML, Hossain MS. Protective effect of black seed oil from *N. sativa* against murine cytomegalovirus infection. *International Journal of Immunopharmacology*. 2000;22(9):729-740.
- Chaieb K, et al. Antibacterial activity of Thymoquinone, an active principle of *N. Sativa* and its potency to prevent bacterial biofilm formation. *BMC Complementary and Alternative Medicine*. 2011;11(1):29.
- Chowdhury AA, et al. Therapeutic potential of the volatile oil of *N. Sativa* seeds in monkey model with experimental shigellosis. *Phytotherapy Research: An International Journal Devoted to Pharmacological and Toxicological Evaluation of Natural Product Derivatives*. 1998;12(5):361-363.

25. Mahmoud M, El-Abhar H, Saleh S. The effect of *N. sativa* oil against the liver damage induced by *Schistosoma mansoni* infection in mice. *Journal of Ethnopharmacology*. 2002;79(1):1-11.
26. Ghannadi A, Hajhashemi V, Jafarabadi H. An investigation of the analgesic and anti-inflammatory effects of *N. sativa* seed polyphenols. *Journal of Medicinal Food*. 2005;8(4):488-493.
27. Marsik P, et al. *In vitro* inhibitory effects of thymol and quinones of *N. sativa* seeds on cyclooxygenase-1-and-2-catalyzed prostaglandin E2 biosyntheses. *Planta Medica*. 2005;71(08):739-742.
28. Shaterzadeh-Yazdi H, et al. Immunomodulatory and Anti-inflammatory Effects of Thymoquinone. *Cardiovascular and Haematological Disorders-Drug Targets (Formerly Current Drug Targets-Cardiovascular and Hematological Disorders)*. 2018;18(1):52-60.
29. Kalus U, et al. Effect of *N. sativa* (black seed) on subjective feeling in patients with allergic diseases. *Phytotherapy Research*. 2003;17(10):1209-1214.
30. Nikakhlagh S, et al. Herbal treatment of allergic rhinitis: The use of *N. sativa*. *American Journal of Otolaryngology*. 2011; 32(5):402-407.
31. Kumara SSM, Huat BTK. Extraction, isolation and characterisation of antitumor principle, α -hederin, from the seeds of *N. sativa*. *Planta Medica*. 2001;67(01):29-32.
32. Nagi MN, Almakki HA. Thymoquinone supplementation induces quinone reductase and glutathione transferase in mice liver: Possible role in protection against chemical carcinogenesis and toxicity. *Phytotherapy Research*. 2009;23(9):1295-1298.
33. Salomi M, Nair SC, Panikkar K. Inhibitory effects of *N. sativa* and saffron (*Crocus sativus*) on chemical carcinogenesis in mice; 1991.
34. Abdel-Wahhab M, Aly S. Antioxidant property of *N. Sativa* (black cumin) and *Syzygium aromaticum* (clove) in rats during aflatoxicosis. *Journal of Applied Toxicology*. 2005;25(3):218-223.
35. Houghton PJ, et al. Fixed oil of *N. sativa* and derived thymoquinone inhibit eicosanoid generation in leukocytes and membrane lipid peroxidation. *Planta Medica*. 1995;61(01):33-36.
36. Haq A, et al. Immunomodulatory effect of *N. sativa* proteins fractionated by ion exchange chromatography. *International Journal of Immunopharmacology*. 1999; 21(4):283-295.
37. Gasteiger E, et al. Protein identification and analysis tools on the ExPASy server. Springer; 2005.
38. Tamura K, Stecher G, Kumar S. MEGA11: Molecular evolutionary genetics analysis version 11. *Molecular Biology and Evolution*. 2021;38(7):3022-3027.
39. Buchan DW, Jones DT. The PSIPRED protein analysis workbench: 20 years on. *Nucleic acids Research*. 2019;47(W1): W402-W407.
40. Combet C, et al. NPS@: Network protein sequence analysis. *Trends in Biochemical Sciences*. 2000;25(3):147-150.
41. Waterhouse A, et al. SWISS-MODEL: Homology modelling of protein structures and complexes. *Nucleic Acids Research*. 2018;46(W1):W296-W303.
42. Laskowski RA, et al. PROCHECK: A program to check the stereochemical quality of protein structures. *Journal of Applied Crystallography*. 1993;26(2):283-291.
43. Sippl MJ. Recognition of errors in three-dimensional structures of proteins. *Proteins: Structure, Function, and Bioinformatics*. 1993;17(4):355-362.
44. Wiederstein M, Sippl MJ. ProSA-web: Interactive web service for the recognition of errors in three-dimensional structures of proteins. *Nucleic Acids Research*. 2007;35(suppl_2):W407-W410.
45. Studio D. Discovery studio. Accelrys [2.1]; 2008.
46. O'Boyle NM, et al. Open Babel: An open chemical toolbox. *Journal of Cheminformatics*. 2011;3(1):1-14.
47. Dallakyan S, Olson AJ. Small-molecule library screening by docking with PyRx. *Chemical biology: Methods and Protocols*. 2015;243-250.
48. Kasahara K, et al. myPresto/omegagene: A GPU-accelerated molecular dynamics simulator tailored for enhanced conformational sampling methods with a non-Ewald electrostatic scheme. *Biophysics and Physicobiology*. 2016; 13:209-216.
49. DeLano WL. Pymol: An open-source molecular graphics tool. *CCP4 Newsl. Protein Crystallogr*. 2002;40(1):82-92.

50. Pires DE, Blundell TL, Ascher DB. pkCSM: Predicting small-molecule pharmacokinetic and toxicity properties using graph-based signatures. *Journal of Medicinal Chemistry*. 2015;58(9):4066-4072.
51. Lipinski CA, et al., Experimental and computational approaches to estimate solubility and permeability in drug discovery and development settings. *Advanced Drug Delivery Reviews*. 2012; 64:4-17.
52. Ghose AK, Viswanadhan VN, Wendoloski JJ. Prediction of hydrophobic (lipophilic) properties of small organic molecules using fragmental methods: An analysis of ALOGP and CLOGP methods. *The Journal of Physical Chemistry A*. 1998; 102(21):3762-3772.
53. Ghose AK, Viswanadhan VN, Wendoloski JJ. A knowledge-based approach in designing combinatorial or medicinal chemistry libraries for drug discovery. 1. A qualitative and quantitative characterization of known drug databases. *Journal of Combinatorial Chemistry*. 1999;1(1):55-68.
54. Veber DF, et al. Molecular properties that influence the oral bioavailability of drug candidates. *Journal of Medicinal Chemistry*. 2002;45(12):2615-2623.
55. Egan WJ, Merz KM, Baldwin JJ. Prediction of drug absorption using multivariate statistics. *Journal of Medicinal Chemistry*. 2000;43(21):3867-3877.
56. Ranjith D, Ravikumar C. SwissADME predictions of pharmacokinetics and drug-likeness properties of small molecules present in *Ipomoea mauritiana* Jacq. *Journal of Pharmacognosy and Phytochemistry*. 2019;8(5):2063-2073.
57. Martin YC. A bioavailability score. *Journal of Medicinal Chemistry*. 2005;48(9):3164-3170.
58. Baell JB, Holloway GA. New substructure filters for removal of pan assay interference compounds (PAINS) from screening libraries and for their exclusion in bioassays. *Journal of Medicinal Chemistry*. 2010;53(7):2719-2740.
59. Brenk R, et al. Lessons learnt from assembling screening libraries for drug discovery for neglected diseases. *ChemMedChem: Chemistry Enabling Drug Discovery*. 2008;3(3):435-444.
60. Teague SJ, et al. The design of leadlike combinatorial libraries. *Angewandte Chemie International Edition*. 1999;38(24): 3743-3748.
61. Grob S. *Slovakia*. Molinspiration Cheminformatics Free Web Services; 2021
Available: <https://www.molinspiration.com> (accessed on 15 January 2022).
62. Banerjee P, et al. ProTox-II: A webserver for the prediction of toxicity of chemicals. *Nucleic Acids Research*. 2018;46(W1): W257-W263.
63. Borba JV, et al. SToxTox: An in silico alternative to animal testing for acute systemic and topical toxicity. *Environmental Health Perspectives*. 2022; 130(2):027012.
64. Anighoro A. Underappreciated chemical interactions in protein–ligand complexes. *Quantum Mechanics in Drug Discovery*. 2020;75-86.
65. Mandlik V, Bejugam PR, Singh S. Application of artificial neural networks in modern drug discovery, in *Artificial neural network for drug design, delivery and disposition*. Elsevier. 2016;123-139.
66. Eslami N, et al. SARS-CoV-2: Receptor and co-receptor Tropism Probability. *Current Microbiology*. 2022;79(5):133.

Disclaimer/Publisher's Note: The statements, opinions and data contained in all publications are solely those of the individual author(s) and contributor(s) and not of the publisher and/or the editor(s). This publisher and/or the editor(s) disclaim responsibility for any injury to people or property resulting from any ideas, methods, instructions or products referred to in the content.

© Copyright (2024): Author(s). The licensee is the journal publisher. This is an Open Access article distributed under the terms of the Creative Commons Attribution License (<http://creativecommons.org/licenses/by/4.0>), which permits unrestricted use, distribution, and reproduction in any medium, provided the original work is properly cited.

Peer-review history:

The peer review history for this paper can be accessed here:

<https://www.sdiarticle5.com/review-history/117584>